Optical Flow Based Background Oriented Schlieren for Compressible Flows

B. O. Cakir[1,2,*], S. Lavagnoli[1], B.H. Saracoglu[1], C. Fureby[2]

1: Dept. of Turbomachinery and Propulsion, von Karman Institute for Fluid Dynamics, Belgium
2: Dept. of Energy Sciences, Lund University, Sweden
*Corresponding author: bora.orcun.cakir@vki.ac.be

Keywords: Compressible flows, Quantitative Visualization, BOS, Optical flow, Wavelet Noise

ABSTRACT

Optical flow provides an opportunity to elevate the resolution and sensitivity of deflection sensing in background oriented schlieren (BOS). Despite extensive relevant literature within the field of computer vision, with regards to BOS, there is a lack of proper quantification of its abilities and limitations. Thus, this study performs a comparative assessment characterizing accuracy and resolution limits in different flow field scenarios utilizing background patterns generated with speckle and wavelet noise distributions. Accordingly, a synthetic assessment over direct numerical simulations of a buoyancy driven turbulence is performed with variations introduced in the background patterns and operational parameters of optical flow where a clear superiority of accuracy and resolvable range of density gradient amplitudes over cross-correlation is demonstrated. Moreover, an experimental assessment of supersonic flow features over multiple models is conducted to characterize the influence of experimental considerations related to the application of optical flow in BOS and its comparative performance against the block-matching counterpart.

1. Introduction

Background oriented schlieren imaging (BOS) is of great interest to fluid dynamics researchers enabling quantitative characterization of density varying flows by means of an inexpensive and simple setup that can be utilized for both two and three-dimensional applications. It is performed by acquiring a pair of images in the presence of density variations occurring in a flow field. These images contain randomly distributed illumination artifacts whose positions on the image plane are modified by the presence of a density varying medium between the recorded scene and the image acquisition system (Settles, 2001). As the pair of images is comprised of one undisturbed and one within the presence of density gradients, the observed variations on the background pattern are traced by means of various digital image processing approaches (Hargather et al., 2011). Thus, the requirements of a BOS setup can be as small as a single camera provided that an accurate optical setup is configured (Hargather & Settles, 2010) which makes it a unique measurement technique that achieves direct quantification of flow features with high versatility and applicability to a wide range of conditions (Raffel et al., 2000).

However, BOS is associated with a major sensitivity limitation originated by an inherent focusing problem (Raffel, 2015). Considering a generic optical configuration for a BOS setup, increasing the sensitivity demands an amplification of the distance between the object and the background while minimizing the distance between the object and the camera. Yet, this is constrained by the increasing errors due to the amplified divergence of the light rays (Elsinga et al., 2004) and geometric blur of the flow features (Gojani et al., 2013). Thus, an inevitable trade-off between the sensitivity and the resolution of the flow structures exists from an optical point of view. On the order hand, the sensitivity and resolution of a BOS system is also governed by the image processing method. Conventionally, the cross-correlation algorithm developed for particle image velocimetry (PIV) (Westerweel, 1997) is used which provides a vector field where the refractive index variations are averaged within interrogation windows (IW) (Keane & Adrian, 1992). Since the minimum size of the IWs is limited to achieve the necessary signal-to-noise ratios (SNR), the resolution of resulting vector field becomes constrained not only by the number of pixels within the IW but also by the intensity of the gradient information being prone to oversmoothing due to the averaging effects (Hargather & Settles, 2012).

Nevertheless, this problem can be addressed by employing optical flow (OF) based image processing techniques (Davies, 2012). Accordingly, Atcheson et al. (2009) demonstrated the possible improvements in BOS measurements over cross-correlation provided by the one 1 vector/pixel reconstruction of displacement fields. Thus, leveraging from its elevated sensitivity and resolution characteristics, various researchers has opted for OF as the deflection sensing method of choice for quantifying the density variations via BOS. Nicolas et al. (2017) performed 3D reconstruction of a supersonic jet flow with a Lucas-Kanade OF approach which also preserved a certain level of neighborhood dependence to solve the closure problem of OF. Hayasaka et al. (2016) used a variational formulation of OF to characterize laser induced underwater shock waves where their approach utilized the residuals of brightness constancy assumption (non-zero divergence) to detect the shockwave shape and location. Furthermore, OF is also utilized for BOS measurements in the presence of reactive flows for performed tomographic reconstruction of flames (Grauer et al., 2018).

Moreover, as the BOS measurements are increasingly employed for the development and validation studies of computational fluid dynamics models (Ramanah et al., 2007; Kirmse et al., 2011), the cross-correlation based BOS approaches become vulnerable to fall short of the corresponding resolution and accuracy requirements while OF is showcased the be a viable solution. Nonetheless, despite its utilization in various occasions, there exits a lack of quantitative characterization of its capabilities and application details especially in high speed compressible flows. Although Heineck et al. (2021) performed natural BOS through in-flight measurements using OF, its capabilities are only demonstrated qualitatively against cross-correlation. Considering the complexity of the models exposed to high speed flows, intensity of the localized density gradients and the varying scales of flow structures, this study showed that OF provides a great opportunity to recover high fidelity density field data from quantitative visualization of supersonic/hypersonic flows. Yet, its utilization requires proper quantification of the resolution, sensitivity and accuracy characteristics of OF based BOS and the associated experimental and image processing considerations. Therefore, this study aims to quantify the accuracy characteristics of optical flow as the deflection sensing stage of BOS compared to cross-correlation where high resolution DNS datasets and various models exposed to supersonic flows in experimental conditions demonstrate the configuration details and the corresponding applicability considerations associated with its employment.

2. Optical flow based BOS

2.1. Optical Flow

Various approaches to OF analysis can be broadly distinguished into two different groups; gradient based and variational algorithms. The common point of these methods is the brightness constancy assumption (Eq.1) where the intensity of pixels moving within the image plane are assumed to be constant (Kearney et al., 1987).

$$\begin{aligned} I(x,y,t) &= I(x+\delta x, y+\delta y, t+\delta t) \\ &= I(x,y,t) + I_t + \delta x I_x + \delta y I_y \end{aligned} \tag{1}$$

Following a gradient based approach, the displacement (δ_x, δ_y) of normalized illumination intensities (I) can be represented as functions of the temporal (I_t) and spatial pixel intensity gradients (I_x, I_y). Nevertheless, underdetermined structure of the resultant governing equation set requires a problem closure to obtain a unique solution which leads to the well known aperture problem (Galvin et al., 1998). Hence, gradient based schemes contain additional energy functions (Eq.2) which include quadratic penalization (ρ_D, ρ_S) of the displacement vector residuals, enforcing brightness constancy proposed by Horn & Schunck (1981). Furthermore, the function to be minimized also contains a penalty contribution from the displacement vector gradients for enhanced robustness while the weighting between the two terms are controlled by a regularization parameter, λ.

$$E(\delta x, \delta y) = \sum \left[\rho_D(I(t+\delta t) - I(t)) + \lambda \rho_S(\nabla \delta x, \nabla \delta y)\right] \tag{2}$$

Moreover, an accurate OF estimation requires adequate handling of the global incoherence and large gradients of displacement vectors. However, as the gradient based formulation relies on small displacements in absence of any discontinuities, additional methods are required to relax the constraints on displacement magnitudes to allow large displacements within the image plane to be reconstructed accurately (Adelson & Bergen, 1985). Accordingly, hierarchical algorithms are proposed to separate the computation of displacement vectors based on the scales of OF contained within the image plane (Anandan, 1989). The acquired images are assumed to contain a wide spatial-frequency spectrum which is decomposed to its bandwidth limited components by means of a pyramid scheme to prevent any loss of resolution or detail (Burt, 1981).

2.2. BOS background generation

The conventional background patterns in BOS are adjusted to suit the needs of the cross-correlation approach to have a high SNR in correlation maps which yielded speckle patterns based on the optical configuration of the measurement system (Fig.1). Accordingly, concentration, size, intensity profile and interparticle distance of the speckles are specified to enable greatest contrast, minimize peak-locking and maximize subpixel accuracy (Adrian & Westerweel, 2011). Alternatively, in line with the sequential downsampling of images following a coarse-to-fine resolution layout, multi-scale procedural noise patterns can be used as the background image to avoid the short comings of random noise functions which often requires a match between the camera resolution and the background pattern for optimum performance (Yang et al., 2014).

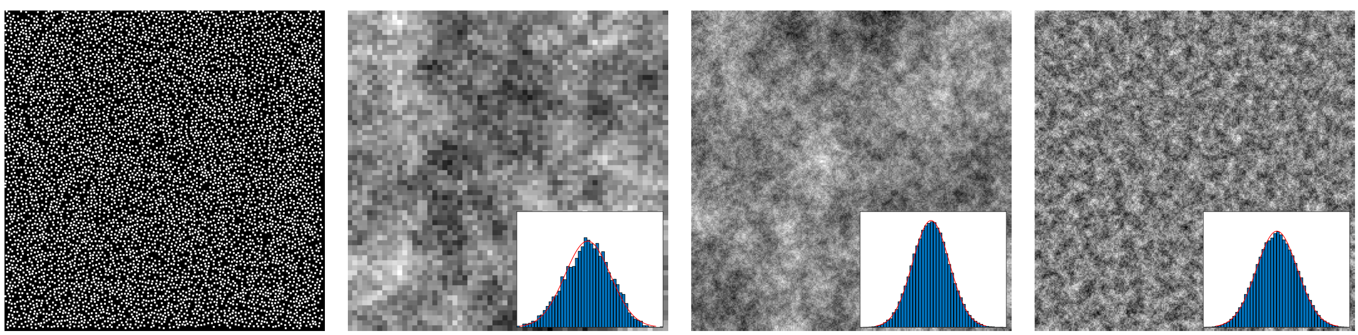

Figure 1. Various background layouts with random dot pattern (left), wavelet noise pattern (n_I,n_F)=(2,5)(mid-left), (n_I,n_F)=(2,8) (mid-right) and (n_I,n_F)=(5,8) (mid-right).

Hence, the wavelet noise (WN) pattern proposed by Cook & DeRose (2005) is utilized to construct a background image where the scaling factors of the hierarchical OF algorithm is matched to capture both large and small scale structures in high accuracy. The content stored within these WN patterns is controlled by means of two parameters, 2^{n_I} (initial resolution) and 2^{n_F} (final resolution). The lower spatial frequency content is modulated by the lower resolution levels where large scale displacements are resolved. This also acts as a anti-aliasing filter when the hierarchical approaches of the OF downsamples the high-resolution image to a lower resolution by preserving orthogonality. Hence, combined with the high frequency content governed by the final resolution specification, each resolution level of noise represents a bandwidth limited procedural texture that can be controlled to the specific spatial resolution needs of the experimental setup. Accordingly, Fig.1 shows three different configurations of WN patterns. Absence of high-frequency content, when the final resolution level (n_F) is decrease, is shown in Fig.1 (mid-left) which disturbs the orthogonality of the noise pattern while removing the low-frequency content. Contrarily, increasing the initial resolution level (n_I), amplifies standard deviation of the intensity distribution where vulnerability against aliasing is increased (Fig.1, right).

3. Synthetic Assessment

Comparative performance characterization of cross-correlation (XCOR) and OF algorithms with different background patterns is performed using a direct numerical simulation (DNS) data of homogeneous buoyancy-driven turbulence (Livescu & Ristorcelli, 2008). Density gradients at the central plane of the 3D simulation volume is extruded to create a constant refractive index field along the line-of-sight which is compatible with a planar BOS application. Then, the ray displacements due to the density variations are rendered via a ray-tracing based image generation methodology (Rajendran et al., 2019). The synthetic optical setup is configured such that a maximum displacement value of 2 pixels is obtained in order to match the dynamic range of XCOR. In consideration of the well-established rules of cross-correlation, the random dot (RD) backgrounds are generated to suit the needs for a high-accuracy reconstruction of displacements using IW sizes of 16x16 pix^2. The dots are arranged to have a Gaussian intensity distribution for high accuracy sub-pixel interpolations which is also in agreement with the spatio-filtering requirements of optical flow (Christmas, 2000). Furthermore, in order to investigate the influence of various spatial frequency ranges contained in the WN patterns, different backgrounds with varying high- and low-frequency levels are generated as shown in Fig.1. The influence of WN backgrounds on the uncertainty levels is quantified by sampling each noise pattern 50 times and providing an additive Gaussian noise to stimulate experimental imperfections prior to being warped with the displacement fields computed from the DNS data (Cai et al., 2022).

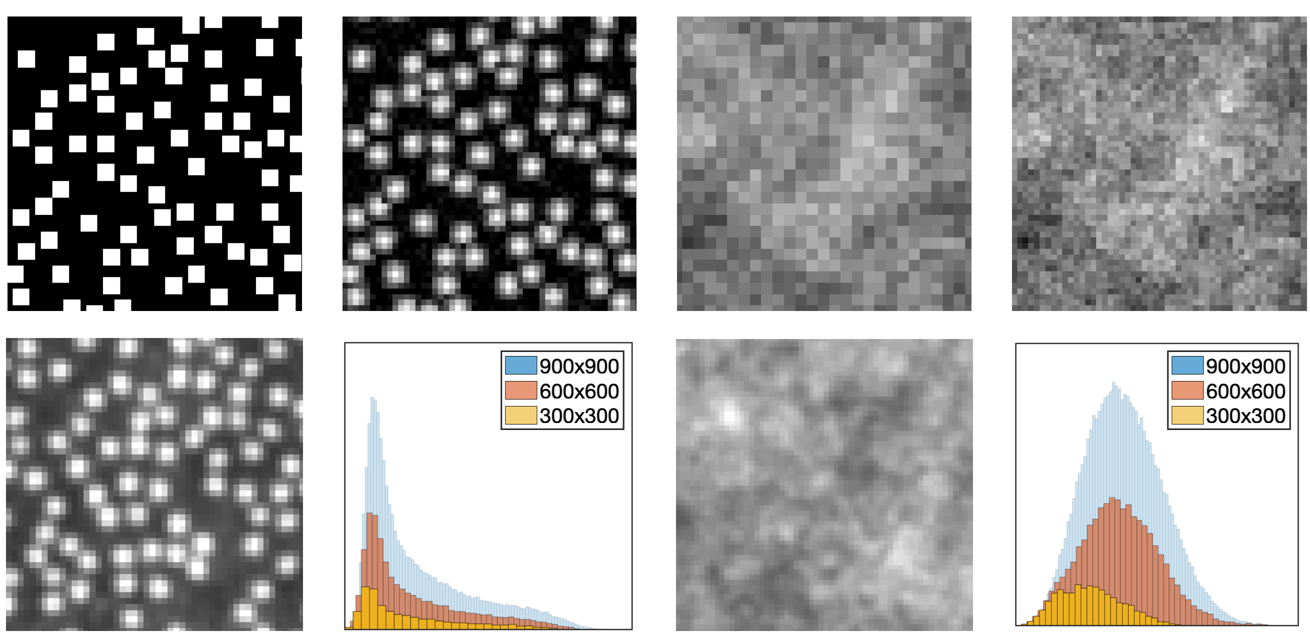

Figure 2. Random dot (left block) and wavelet noise (right block) backgrounds; computer generated pattern (top-left quadrant), synthetically modified pattern (top-right quadrant), experimentally acquired image (bottom-left quadrant) and histograms of illumination intensity at three different sampling levels (bottom-right quadrant).

While both types of backgrounds are utilized for assessing the accuracy of OF, only the RD backgrounds are used with XCOR due to the downgraded SNR of the correlation maps caused by the reduced contrast of the WN pattern (Atcheson et al., 2008). The Horn-Shunck OF (described in Sec.2) is employed through an open-source computer vision (CV) code by Sun et al. (2014). The hierarchical layout is constructed using 6 pyramid levels to minimize the interpolation error between different levels (Hofinger et al., 2020) and 10 intermediate warping steps based on a convergence criteria of 10^{-2} of the intermediate energy function residuals. For each background configuration, the regularization parameter is varied over a range ($0.01 \leq \lambda \leq 250$) to demonstrate the influence of different weighting schemes. Moreover, XCOR is performed using a multi-pass approach where 3 passes with consecutive reduction of IW sizes (64×64, 32×32, 16×16 pix^2) is employed with 50% overlap (Thielicke & Sonntag, 2021). Finally, the obtained results using various methods are compared both qualitatively and quantitatively over the average end-point errors (AEPE) (Baker et al., 2007) of dedicated regions indicated in Fig.3 (top-middle), and the resolution range of the spatial frequency spectrum.

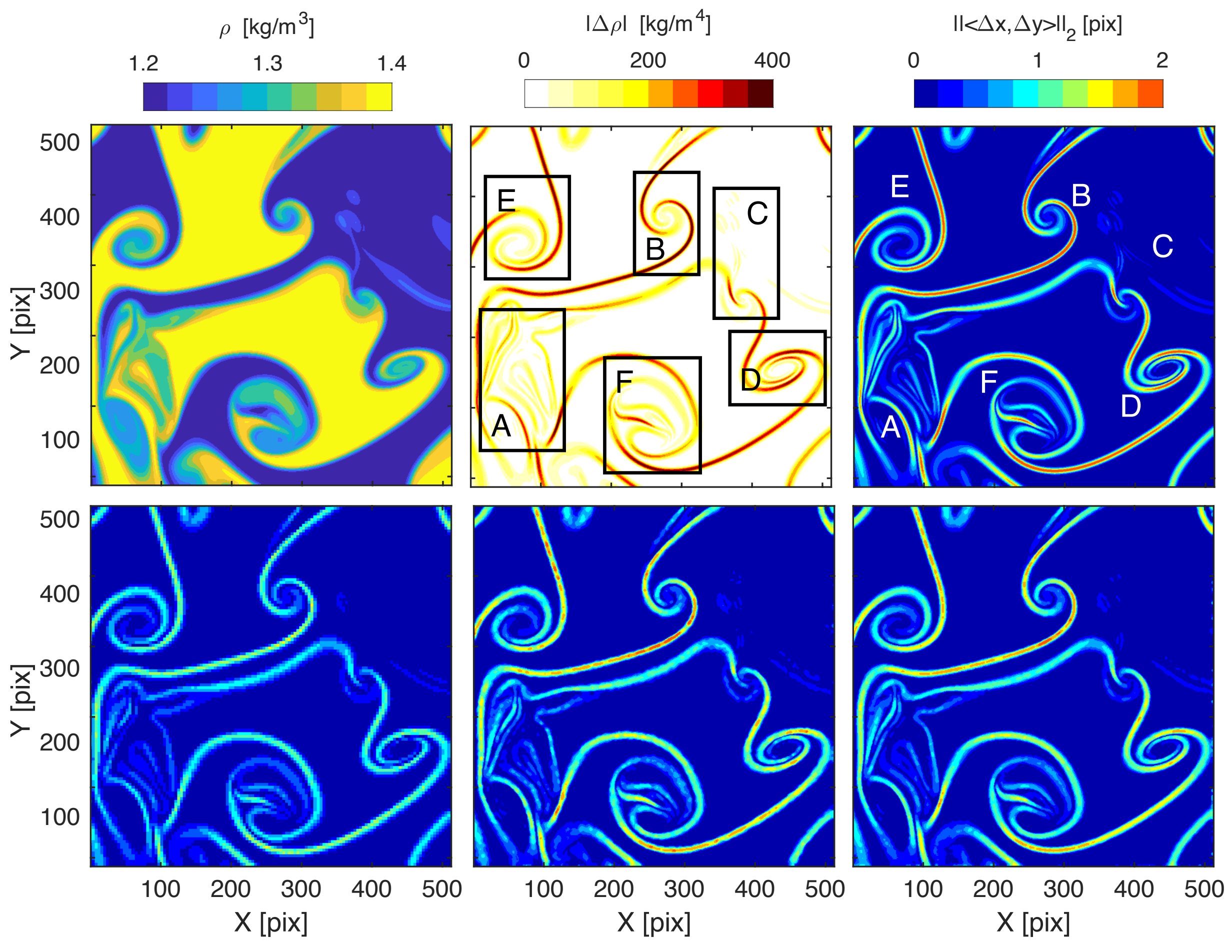

Figure 3. DNS density field (top-left), DNS density gradients (top-middle), reference displacement magnitude (top-right), displacement magnitudes obtained with cross-correlation (bottom-left), OF with random dot (bottom-middle) and wavelet noise (bottom-right) backgrounds.

To start with the qualitative assessments, the resolution superiority (0.0625 vector/pixel (XCOR) vs. 1 vector/pixel (OF)) of OF inherently allows higher sensitivity in terms of the gradients of displacement vectors. Regardless of the background type, OF is able to capture larger displacement regions with improved accuracy as XCOR suffers from the averaging effect over the locally confined presence of density gradients which causes the displacements to be dissipated over larger local regions (Fig.3). Nevertheless, the spatial dependency allows XCOR to be free of local spurious vectors while OF suffers slightly from local noise which is caused by the vulnerability associated with increased sensitivity. Furthermore, comparing the performance of OF with RD and WN backgrounds, the increased level of noise is noticeable with the use of RD backgrounds. This is related to the fact that, in absence of illumination distributions induced by dots, OF is left with the low level additive noise on the images to trace the displacements. Thus, WN backgrounds covering the entire image plane with a controlled intensity variation prevents the dependence of the reconstruction procedure on the random distribution of dots and increases the consistency of the reconstruction accuracy. However, the consistency is traded off with loss of accuracy in some regions where a better match between the reconstructed displacement field and the reference is obtained with RD backgrounds due to the higher contrast levels.

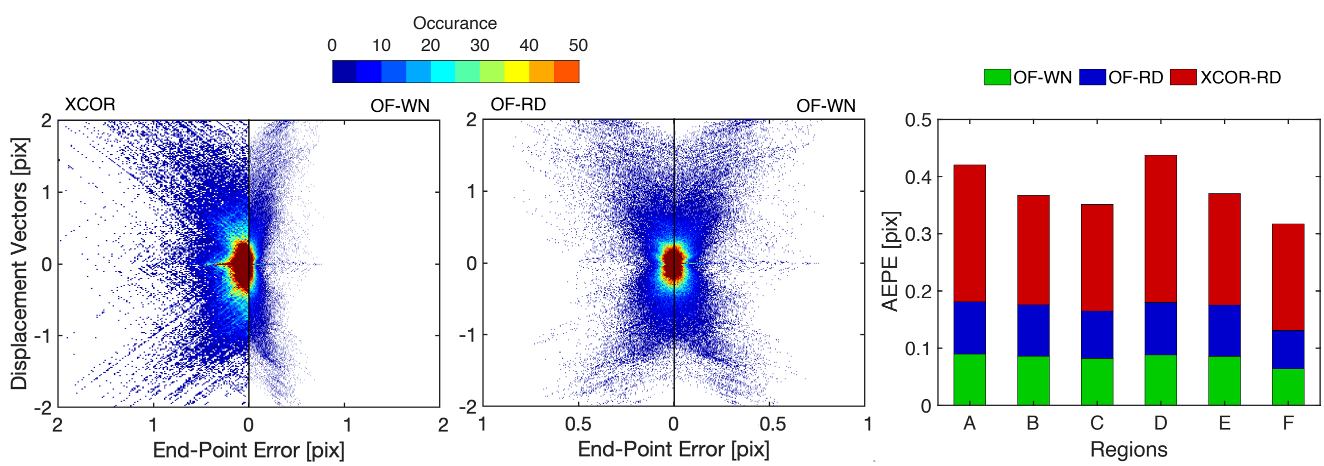

Figure 4. 2D histograms of end-point errors with reference displacement vectors; XCOR vs OF-WN (left) and OF-WN vs OF-RD (middle). Average end-point errors over the designated regions with XCOR, OF-WN and OF-RD (right).

Characterizing the resolvable spatial frequency range, Fig.4 (left) demonstrates the distribution of reconstruction errors with respect to the magnitude of the displacement vector components they are associated with. In case of XCOR, the erroneous vectors tend to increase their amplitude in correlation increasing displacement which reveals a more dispersed layout in the histogram plot. This is owing to the highly localized existence of density gradients within the DNS flow field and the incapability of XCOR to capture them with high accuracy due to the spatial averaging characteristics. On the other hand, the hierarchical reconstruction scheme of OF, bounds the errors to a lower range which are observed to be independent of the displacement vector magnitude. Thus, the superior capability of OF to have the same level of accuracy throughout the entirety of the spatial frequency spectrum when used in a multi-resolution layout is apparent. Moreover, dominance of the processing algorithm in comparison to the background in use is further indicated by Fig.4 (middle) where a strong match between the error distributions obtained with OF using both RD and WN backgrounds is present. Thus, computation of AEPE over the identified regions further supports these results where accuracy superiority of OF over XCOR is clear by an average of 75% reduction in error magnitudes with both background patterns (Fig.4, right).

Furthermore, a parametric study on the influence of background patterns is performed with varying initial (n_I) and final (n_F) resolution levels of the WN pattern. First, the initial spatial resolution level is kept constant at the minimum level (n_I=2) while the final resolution level is modified ($5 \leq n_F \leq 10$). Due to the high resolution characteristics of the DNS data with extremely localized large magnitude displacement values, an increase of accuracy with increasing n_F is noted. The minimum error for reconstruction is obtained at the level of n_F=8 which matched the downsampled resolution DNS to stimulate the defocusing effect from the flow field associated with BOS setups (Fig.5, left). This due to the fact that, as the final resolution level is increased beyond the resolution of the flow field, the contribution of the displacements caused by the flow field are suppressed. Hence, increasing the regularization parameter shifted the influence of displacement gradients to the lower end of the spatial frequency spectrum which yielded lower reconstruction accuracy for $n_F \geq 9$. Then the procedure for background generation is inverted by keeping the final resolution level at n_F=8 and varying the initial resolution level over a range of $2 \leq n_I \leq 5$ (Fig.5, middle). The impact of modifying the lower end of the spatial frequency spectrum is observed to be significantly small compared to the n_F which is attributed to the characteristics of the DNS case where density gradients are considerably localized. Thus, having the correct range of resolution (n_I=2 & n_F=8) levels where the motion over image plane is dominated by the displacement vectors, allows OF to resolve the full spectrum of spatial frequency domain. Moreover, increasing the initial resolution level influences the uncertainty levels of the OF reconstructions by increasing the possibility of aliasing due to the removal of lower frequency content.

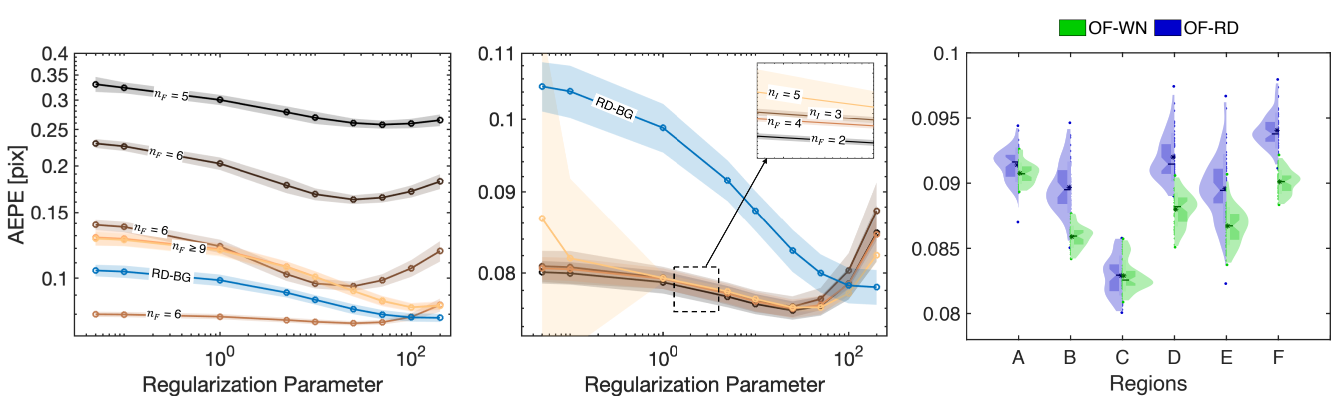

Figure 5. Average end-point errors obtained with optical flow using various wavelet noise patterns; variation of final resolution while $n_I = 2$ (left) and variation of initial resolution while $n_F = 8$ (middle). Blue line refers to the Average end-point errors obtained with optical flow using random dot patterns. Average end-point errors over the designated regions with OF-WN and OF-RD (right).

Finally, analyzing the influence of regularization parameter on the OF reconstructions using RD backgrounds, higher levels of regularization parameters is required to achieve higher accuracy. This is also related to the same contrast issue over the regions that suffer from the scarcity of dots where the considerably low level of illumination intensities (associated with the additive noise) provides the only artifacts that OF can use to trace the motion of the background pattern. Accordingly, the spatial accuracy consistency of WN backgrounds over RD backgrounds is denoted in Fig. 5 (right) in terms of error distributions throughout the designated regions. The error levels are not only lower with WN backgrounds but they are also confined lower ranges whereas with RD backgrounds the manifold of the error distributions throughout the identified regions are larger. Thus, a high confidence reconstruction of ray displacements over a wider range of density gradient amplitudes can be established with optical flow especially coupled with a procedural noise pattern that contains multiple levels of spatial-frequency scales. On the other hand, the limited dynamic range of cross-correlation due to bandwidth filtering, causes loss of detail and accuracy.

4. Experimental Assessment

The experimental setup employed in this work is implemented on the S-4 supersonic wind tunnel of von Karman Institute (VKI) which is a blown-down wind tunnel equipped with a 2D contoured nozzle providing Mach 3.5 supersonic flow into a test section of 8×10 cm^2. Configuration of the BOS setup is composed of a Hamamatsu ORCA-Flash4.0 V3 Digital CMOS camera, a f = 200 mm Nikkor lens, four Chazon 100W 10x10 LED arrays as the light source and backgrounds laser printed on 240 g/m^2 paper (Fig.6 & Fig.7). The backgrounds are illuminated from the behind to enhance the recorded contrast and remove reflection effects. The distance between the light source and the background is adjusted to optimize the trade-off between light intensity and uniformity. Two different models of a von Karman ogive and a 10^o wedge (end-to-end) are utilized for the tests to have a wide range of density gradients as well as comparing two and three dimensional flow features. The selection of the backgrounds containing RD and WN patterns are both tailored to suit the specifications of the optical configuration dictated by the requirements of the XCOR approach while the WN backgrounds are generated according to the parametric study performed in Sec.3 respectively. Finally, 40 wind-on images for each model and background combination are recorded with an acquisition frequency of f_{aq}=10Hz using an aperture of $f_{\#}$=22 to minimize the defocusing effects of blur and diffraction in the vicinity of model surface (Tab.1).

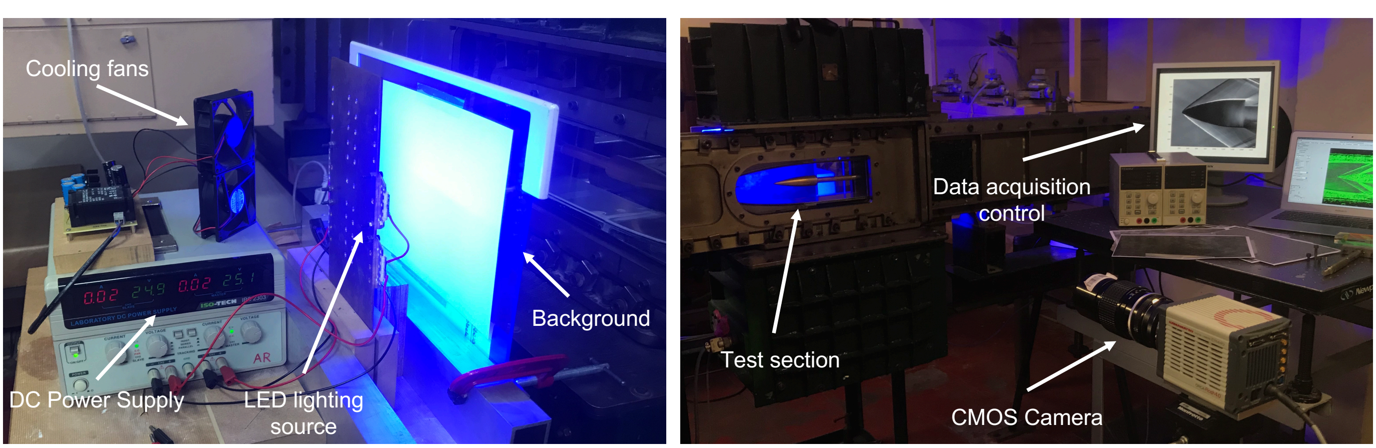

Figure 6. Experimental setup of the background oriented schlieren system in the S-4 supersonic wind tunnel of VKI.

Analyzing the reconstructed structures of the supersonic flows over the two models, a strong conical shockwave is observed to be attached at the nose of the ogive (Fig.8, top). Due to the relaxation of the surface tangent over a von Karman ogive, weak expansion waves are generated over the surface of the model that impinge on the conical shock. Hence, the corresponding reduction in the intensity of the shock with constant upstream conditions is associated with the shock becoming less steeper further away from the model (Dolling & Bogdonoff, 1979). On the other hand, the oblique shock attached at the leading edge of the wedge is observed to be on a straight line due to the planar structure of the 2D wedge. Yet its strength and thickness is increased further away from the model (Fig.8, bottom) owing to the impingement of weak compression waves generated by the modulations on the effective compression surface induced by surface roughness. As the supersonic flow past the leading edge shock proceeds towards the expansion shoulder of the wedge where the flow re-aligns with the incoming stream, a strong expansion fan is generated.

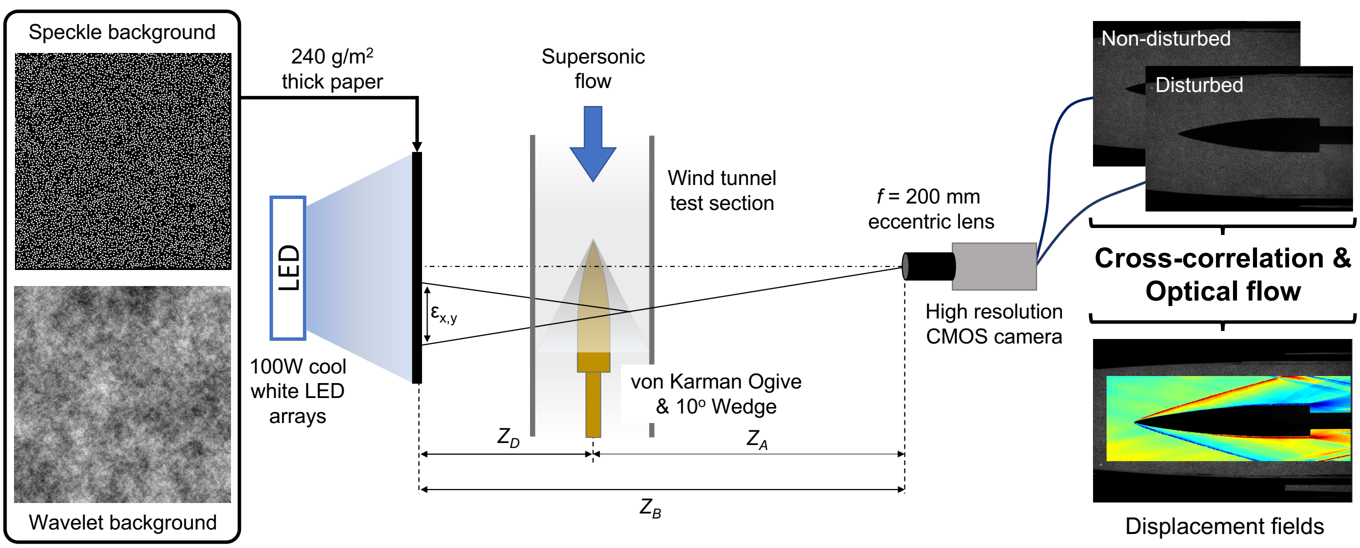

Figure 7. Schematic of the experimental setup with employed pattern of random dot and wavelet noise backgrounds and deflection sensing procedure.

All three approaches are able to visualize the variation of the shock angle further away from the ogive while the increased resolution characteristics of OF enables a clearer identification of the shock location both with RD and WN backgrounds compared to XCOR. Nevertheless, the differences between the utilized reconstruction approaches become more severe when finer details in the weak expansion region over the ogive surface is investigated. Although XCOR is capable of capturing the some of the higher intensity expansion phenomena, weaker waves are vaguely reconstructed (Fig.8, top-left). On the contrary, OF is capable of capturing the vast majority of the weak expansion waves regardless of the amplitude (Fig.8, top-middle & top-right). Furthermore, this situation is also confirmed when the magnitude of the displacements are quantified at various locations over the ogive flow field (Fig.9, middle). The lower resolution of XCOR and the associated spatial smoothing effect causes density gradients confined to small regions to be underestimated. In the case of the ogive, these regions correspond to the vicinity of the shock wave where the displacement magnitudes are not only localized sufficiently to give a precise description of the shock location, but also reconstructed with significantly lower amplitudes compared to OF.

Table 1. Configuration details for the random dot and wavelet noise background patterns, and testing conditions.

Random Dot	N_I [ppp]	d_P [pix]	Δ_P [pix]
	0.027	2.25	5
Wavelet Noise	n_I	n_F	PJ [dpp]
	2	10	21
Setup measures	Z_A [m]	Z_D [m]	Z_B [m]
	2.6	0.2	2.4
Image acquisition	f_{acq} [Hz]	$f_{\#}$	M
	10	22	0.072
Testing Conditions	P_0 [bar]	M_∞	Re [1/m]
	8	3.5	15×10^6

The clarity of the flow features in the base region of the ogive (separated shear layer, the lip shock and the reattachment shock (Van Gent et al., 2019) denotes the increased resolution characteristics of OF against XCOR (Fig.8, top). The improved resolution of finer detail flow structures with OF persists with the employment of the wedge model. The weak compression waves generated over the compression ramp are captured with greater fidelity compared to the XCOR where only mild displacement magnitudes are reconstructed over the ramp region (Fig.9, right). In addition to the resolution limit of XCOR, the bandwidth limited characterization of XCOR restricts the resolvable range of the ray displacements caused by density gradients. Hence, in close range of the expansion shoulder of the wedge, the displacement magnitudes reach to levels of 8 pixels which is above the resolvable limit of 16×16 pix^2 IWs with 50% overlap. Thus, in combination with the spatial smoothing effect where the expansion region is also rather small, the displacements are severely underestimated (Fig.9, middle). Nonetheless, in regions further away from the model where the density gradients are more dispersed, both the larger domain of displacements and the lower amplitude within the dynamic range of the XCOR configuration being used, the displacement vectors are accurately reconstructed (Fig.9, right).

Comparing the performance of different background patterns for OF, WN seem to yield higher noise levels over the displacement maps which interferes with the sensitivity of the density gradients of interest. This effect becomes more effective when finer details in small regions are being analyzed as the increased noise level and the associated errors make identification of small scale structures harder (Fig.8, bottom-middle & bottom-left). The increased noise of reconstruction is related to the changing contrast range at different image pyramid levels (as shown in Fig. 2) while the contrast range of RD backgrounds do not vary when the acquired images are subsampled at

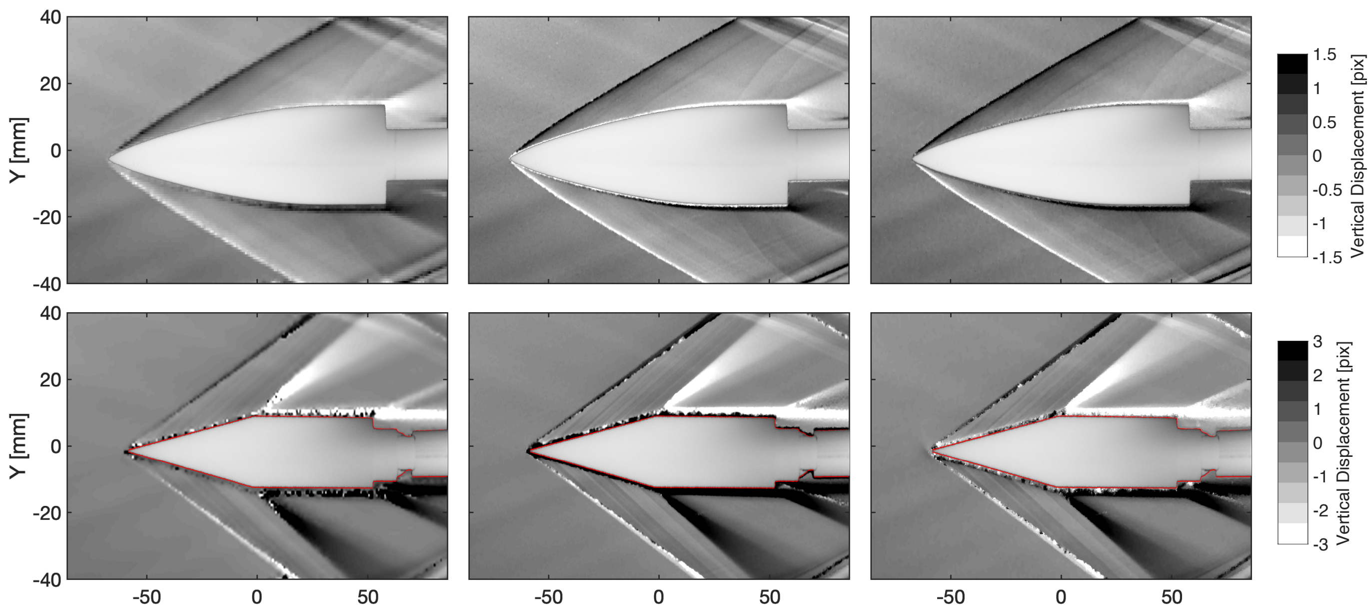

Figure 8. Time averaged vertical displacements for supersonic flow past von Karman ogive (top) and 10^o wedge (bottom) reconstructed with XCOR (left), OF with random dot (middle) and wavelet noise (right) backgrounds.

different levels of resolution. Thus, even though the WN preserved its orthogonality by keeping a Gaussian distribution at every level and region of sampling, the degraded intensity of gradients reduces the confidence level of OF estimation. The loss of contrast is observed to be due to a combination of experimental factors including the quality of the paper the backgrounds are printed on, the printer itself and the light source. Hence, employing a quadratic penalty definition, this situation shifts the influence on the energy function towards the brightness constancy residuals which causes larger amplitudes of small scale spurious structures to occur. Thus, RD backgrounds provide enhanced robustness against these artifacts due to the elevated contrast levels which also suit the formulation of Horn-Shuck OF when diffraction limited images yield circular illumination spots with a Gaussian distribution of intensity variation.

Finally, in order the quantify the physical characteristics of the reconstructed flow structures and the differences achieved with various methods, the physical alignment of the shock waves and expansion fans are computed by identifying locations of higher magnitudes of second order density gradients (Laguarda et al., 2021). Then, for the ogive a 3^{rd} order polynomial is fitted over the identified shock location in order to capture the variations over the shock angle while the leading edge shock and the expansion fan over the wedge model are reconstructed by a linear regression (Fig.9, left). First of all, the OF based reconstructions revealed a greater agreement compared to the XCOR for capturing the conical shock angle at the tip of the ogive due to the better reconstruction characteristics in close proximity of the ogive tip where the displacements are significantly localized. Furthermore, the linearity of the shock owing to the straight contour of the wedge allowed all three approaches to capture the relevant shock angle accurately irrespective of the sensitivity of reconstructions in close proximity of the model. The slight deviation from the theory for all

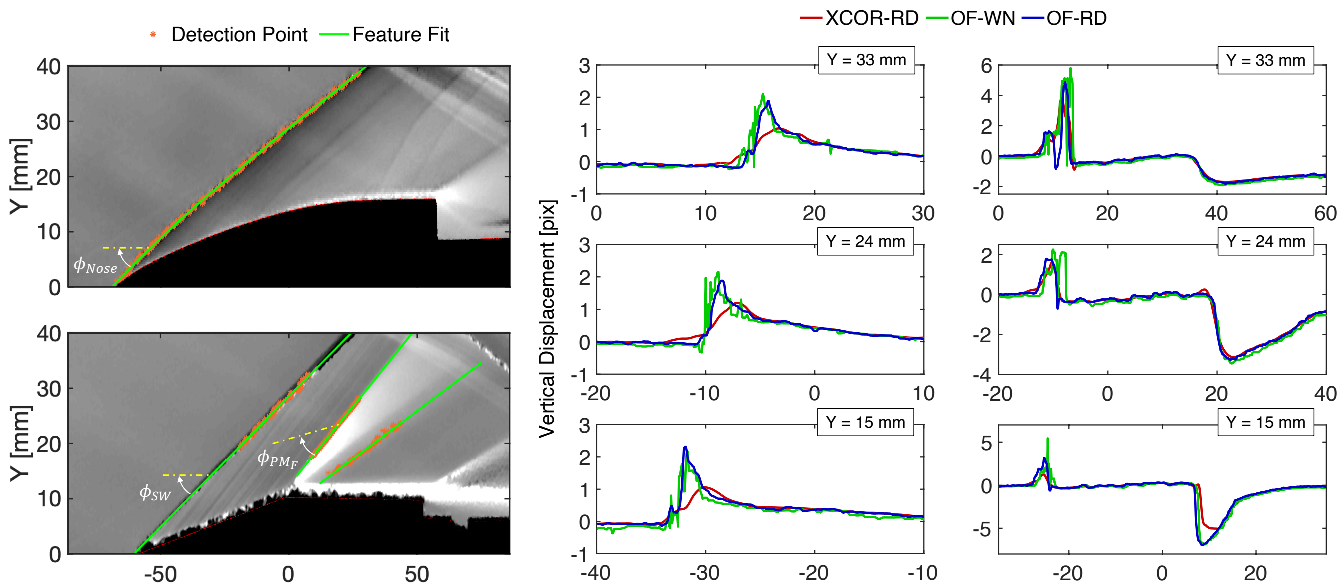

Figure 9. Flow feature detection scheme demonstrated over the ogive (top-left) and 10^o wedge (bottom-left). Extracted time averaged vertical displacement magnitudes over the flow fields of ogive (middle) and 10^o wedge (right).

three methods is caused by a small modulation in the angle of attack of the wedge in the negative direction during the wind tunnel operation which caused the upper surface deflection angle to be greater than 10^o. Then, comparing the angle of the 1^{st} Mach wave of the Prandtl-Meyer (PM) expansion fan, the distinctive accuracy of the OF based approaches is again denoted with an accurate detection of the starting position of the expansion fan while XCOR caused the Mach wave angle to be underestimated (Tab.2).

Table 2. Alignment (time average and standard deviation) of featured flow structures for the von Karman ogive and 10^o wedge with the local flow direction compared against theory.

Ogive	Theory (Sims, 1964)	XCOR-RD	OF-RD	OF-WN
ϕ_{Nose} [deg]	27.8	22.6±1.2	27.6±0.1	27.7±0.2
10^o Wedge	Theory (Anderson, 2001)	XCOR-RD	OF-RD	OF-WN
ϕ_{SW} [deg]	24.4	25.7±0.1	25.2±0.1	25.3±0.1
ϕ_{PM_F} [deg]	20.2	18.9±1.3	20.1±0.1	20.0±0.1

5. Conclusions

Simplicity of application and minimal requirements for its experimental configuration makes background oriented schlieren (BOS) a cost-effective solution for quantitative visualization of density varying flows. Yet, degraded resolution and sensitivity characteristics of BOS outweighs its benefits in comparison to parallel light schlieren systems. In this regard, optical flow (OF) provides a unique opportunity to recover high fidelity density field variations at the deflection detection stage of BOS. Thus, in order to have a full comprehension of its capabilities over the conventional cross-correlation approach and its application considerations, a comparative study including high resolution DNS data of a homogeneous buoyancy driven turbulence and experimental measurements of supersonic flows over various models is conducted. The OF based reconstructions revealed superior characteristics of resolution and sensitivity against XCOR which allowed higher accuracy reconstructions of displacement vectors. The hierarchical schemes enabled OF to resolve the full spatial-frequency spectrum of the displacements contained within the image plane where the bandwidth limited nature of XCOR suffered not only from smoothing due to spatial averaging but also from a limited dynamic range. The influence of varying background patterns and OF configurations is also investigated with wavelet noise that allows the spatial frequency resolution specification of the image pyramids for OF to be complemented. Even though synthetic assessments performed in a controlled environment attributed the greatest accuracy to OF application with procedural background patterns, both in terms of resolution of the spatial-frequency domain and consistency, experimental considerations of various illumination and printing artifacts yielded speckle patterns to be the robust option while multi-scale noise patterns suffered from vulnerability against the noise.

Acknowledgements

The authors would like to thank Dr.Guillaume Grossir from Aerospace and Aeronautics Department of VKI for his insightful comments and invaluable help regarding configuration of the experimental setup. This project has received funding from the European Union's Horizon 2020 research and innovation programme under grant agreement No 101006856.

References

Adelson, E. H., & Bergen, J. R. (1985). Spatiotemporal energy models for the perception of motion. *Journal of the Optical Society of America. A, Optics and image science*, *2 2*, 284-99. doi: 10.1364/JOSAA.2.000284

Adrian, R., & Westerweel, J. (2011). *Particle image velocimetry*. Cambridge University Press.

Anandan, P. (1989). A computational framework and an algorithm for the measurement of visual motion. *International Journal of Computer Vision*, *2*(3), 283-310. doi: 10.1007/BF00158167

Anderson, J. (2001). *Fundamentals of aerodynamics*. McGraw-Hill.

Atcheson, B., Heidrich, W., & Ihrke, I. (2009). An evaluation of optical flow algorithms for background oriented schlieren imaging. *Experiments in Fluids*, *46*(3), 467-476. doi: 10.1007/s00348-008-0572-7

Atcheson, B., Ihrke, I., Heidrich, W., Tevs, A., Bradley, D., Magnor, M., & Seidel, H.-P. (2008). Time-resolved 3d capture of non-stationary gas flows. *ACM Trans. Graph.*, *27*(5). doi: 10.1145/1409060.1409085

Baker, S., Roth, S., Scharstein, D., Black, M. J., Lewis, J., & Szeliski, R. (2007). A database and evaluation methodology for optical flow. In *2007 ieee 11th international conference on computer vision* (p. 1-8). doi: 10.1109/ICCV.2007.4408903

Burt, P. J. (1981). Fast filter transform for image processing. *Computer Graphics and Image Processing*, *16*(1), 20-51. doi: 10.1016/0146-664X(81)90092-7

Cai, H., Song, Y., Ji, Y., Li, Z., & He, A. (2022). Direct background-oriented schlieren tomography using radial basis functions. *Opt. Express*, *30*(11), 19100–19120. doi: 10.1364/OE.459872

Christmas, W. (2000). Filtering requirements for gradient-based optical flow measurement. *IEEE Transactions on Image Processing*, *9*(10), 1817-1820. doi: 10.1109/83.869192

Cook, R. L., & DeRose, T. (2005). Wavelet noise. *ACM Trans. Graph.*, *24*(3), 803–811. doi: 10.1145/1073204.1073264

Davies, E. (2012). Chapter 19 - motion. In *Computer and machine vision (fourth edition)* (Fourth Edition ed., p. 505-522). Boston: Academic Press. doi: 10.1016/B978-0-12-386908-1.00019-7

Dolling, D., & Bogdonoff, S. (1979). *Supersonic, high reynolds number flow over a tangent ogive cylinder at small angles of attack. an experimental study and comparison with theory*. Princeton University, Dept. of Mechanical and Aerospace Engine.

Elsinga, G. E., van Oudheusden, B. W., Scarano, F., & Watt, D. W. (2004). Assessment and application of quantitative schlieren methods: Calibrated color schlieren and background oriented schlieren. *Experiments in Fluids*, *36*(2), 309-325. doi: 10.1007/s00348-003-0724-8

Galvin, B., McCane, B., Novins, K., Mason, D., & Mills, S. (1998). Recovering motion fields: An evaluation of eight optical flow algorithms. In *Proceedings of the british machine vision conference* (p. 20.1-20.10). BMVA Press. doi: 10.5244/C.12.20

Gojani, A. B., Kamishi, B., & Obayashi, S. (2013). Measurement sensitivity and resolution for background oriented schlieren during image recording. *Journal of Visualization*, *16*(3), 201-207. doi: 10.1007/s12650-013-0170-5

Grauer, S. J., Unterberger, A., Rittler, A., Daun, K. J., Kempf, A. M., & Mohri, K. (2018). Instantaneous 3d flame imaging by background-oriented schlieren tomography. *Combustion and Flame*, *196*, 284-299. doi: 10.1016/j.combustflame.2018.06.022

Hargather, M. J., Lawson, M. J., Settles, G. S., & Weinstein, L. M. (2011). Seedless velocimetry measurements by schlieren image velocimetry. *AIAA Journal*, *49*(3), 611-620. doi: 10.2514/1.J050753

Hargather, M. J., & Settles, G. S. (2010). Natural-background-oriented schlieren imaging. *Experiments in Fluids*, *48*(1), 59-68. doi: 10.1007/s00348-009-0709-3

Hargather, M. J., & Settles, G. S. (2012). A comparison of three quantitative schlieren techniques. *Optics and Lasers in Engineering*, *50*(1), 8-17. (Advances in Flow Visualization) doi: 10.1016/j.optlaseng.2011.05.012

Hayasaka, K., Tagawa, Y., Liu, T., & Kameda, M. (2016). Optical-flow-based background-oriented schlieren technique for measuring a laser-induced underwater shock wave. *Experiments in Fluids*, *57*(12), 179. doi: 10.1007/s00348-016-2271-0

Heineck, J. T., Banks, D. W., Smith, N. T., Schairer, E. T., Bean, P. S., & Robillos, T. (2021). Background-oriented schlieren imaging of supersonic aircraft in flight. *AIAA Journal*, *59*(1), 11-21. doi: 10.2514/1.J059495

Hofinger, M., Bulò, S. R., Porzi, L., Knapitsch, A., Pock, T., & Kontschieder, P. (2020). Improving optical flow on a pyramid level. In *Computer vision – eccv 2020* (pp. 770–786). Cham: Springer International Publishing. doi: 10.1007/978-3-030-58604-1_46

Horn, B. K., & Schunck, B. G. (1981). Determining optical flow. *Artificial Intelligence*, *17*(1), 185-203. doi: 10.1016/0004-3702(81)90024-2

Keane, R. D., & Adrian, R. J. (1992). Theory of cross-correlation analysis of piv images. *Applied Scientific Research*, *49*(3), 191-215. doi: 10.1007/BF00384623

Kearney, J. K., Thompson, W. B., & Boley, D. L. (1987). Optical flow estimation: An error analysis of gradient-based methods with local optimization. *IEEE Transactions on Pattern Analysis and Machine Intelligence*, *PAMI-9*(2), 229-244. doi: 10.1109/TPAMI.1987.4767897

Kirmse, T., Agocs, J., Schröder, A., Martinez Schramm, J., Karl, S., & Hannemann, K. (2011). Application of particle image velocimetry and the background-oriented schlieren technique in the high-enthalpy shock tunnel göttingen. *Shock Waves*, *21*(3), 233-241. doi: 10.1007/s00193-011-0314-2

Laguarda, L., Santiago Patterson, J., Schrijer, F. F. J., van Oudheusden, B. W., & Hickel, S. (2021). Experimental investigation of shock–shock interactions with variable inflow mach number. *Shock Waves*, *31*(5), 457-468. doi: 10.1007/s00193-021-01029-3

Livescu, D., & Ristorcelli, J. R. (2008). Variable-density mixing in buoyancy-driven turbulence. *Journal of Fluid Mechanics*, *605*, 145–180. doi: 10.1017/S0022112008001481

Nicolas, F., Donjat, D., Léon, O., Le Besnerais, G., Champagnat, F., & Micheli, F. (2017). 3d reconstruction of a compressible flow by synchronized multi-camera bos. *Experiments in Fluids*, *58*(5), 46. doi: 10.1007/s00348-017-2325-y

Raffel, M. (2015). Background-oriented schlieren (bos) techniques. *Experiments in Fluids*, *56*(3), 60. doi: 10.1007/s00348-015-1927-5

Raffel, M., Richard, H., & Meier, G. E. A. (2000). On the applicability of background oriented optical tomography for large scale aerodynamic investigations. *Experiments in Fluids*, *28*(5), 477-481. doi: 10.1007/s003480050408

Rajendran, L. K., Bane, S. P. M., & Vlachos, P. P. (2019). PIV/BOS synthetic image generation in variable density environments for error analysis and experiment design. *Measurement Science and Technology*, *30*(8), 085302. doi: 10.1088/1361-6501/ab1ca8

Ramanah, D., Raghunath, S., Mee, D. J., Rösgen, T., & Jacobs, P. A. (2007). Background oriented schlieren for flow visualisation in hypersonic impulse facilities. *Shock Waves*, *17*(1), 65-70. doi: 10.1007/s00193-007-0097-7

Settles, G. S. (2001). Basic concepts. In *Schlieren and shadowgraph techniques: Visualizing phenomena in transparent media* (pp. 25–38). Berlin, Heidelberg: Springer Berlin Heidelberg. doi: 10.1007/978-3-642-56640-0_2

Sims, J. L. (1964). Tables for supersonic flow around right circular cones at zero angle of attack.

Sun, D., Roth, S., & Black, M. J. (2014). A quantitative analysis of current practices in optical flow estimation and the principles behind them. *International Journal of Computer Vision*, *106*(2), 115-137. doi: 10.1007/s11263-013-0644-x

Thielicke, W., & Sonntag, R. (2021). Particle image velocimetry for MATLAB: Accuracy and enhanced algorithms in PIVlab. *Journal of Open Research Software*, *9*. doi: 10.5334/jors.334

van Gent, P. L., Payanda, Q., Brust, S. G., van Oudheusden, B. W., & Schrijer, F. F. J. (2019). Effects of exhaust plume and nozzle length on compressible base flows. *AIAA Journal*, *57*(3), 1184-1199. doi: 10.2514/1.J057314

Westerweel, J. (1997). Fundamentals of digital particle image velocimetry. *Measurement Science and Technology*, *8*(12), 1379–1392. doi: 10.1088/0957-0233/8/12/002

Yang, C., Yao, L., Xu, Z., Chen, X., Liu, J., & Kan, R. (2014). Random dots' parameters optimization study of background for background oriented schlieren (bos) environmental research application. In *Light, energy and the environment* (p. EW4A.6). Optica Publishing Group. doi: 10.1364/E2.2014.EW4A.6